Numerical Simulation of Plasma Processes Driven by Transverse Ion Heating

NAGENDRA SINGH AND C. B. CHAN

Department of Electrical and Computer Engineering, University of Alabama in Huntsville

Numerical simulation is performed to study the plasma processes driven by transverse ion heating in a diverging flux tube. It is found that the heating drives a host of plasma processes, in addition to the well-known phenomenon of ion conics. The additional processes include formation of a density cavity topped by a density enhancement, formation of a reverse and forward shock pair with a "double-sawtooth" structure in the flow velocity. The downward electric field near the reverse shock generates a doublestreaming situation consisting of two upflowing ion populations with different average flow velocities. A double streaming also occurs above the forward shock, where the ions energized by the heating are overtaking the relatively slow ions in the ambient polar wind. The energized ions appear as "elevated" ion conics with a low-energy cutoff depending on the distance from the heating region. The parallel electric fields generated by the transverse ion heating have the following noteworthy features; the electric field near the forward shock is essentially unipolar, and it points upward, and for the heating localized in both space and time, the field has the features of a weak double layer. The electric field in the reverse shock region is modulated by the ion-ion instability driven by the multistreaming ions. The oscillating fields in this region have the possibility of heating electrons. The results from the simulations are compared with results from a previous study based on a hydrodynamic model. Effects of spatial resolutions afforded by simulations on the evolution of the plasma are discussed, demonstrating how a crude resolution can miss out plasma instabilities, affecting the plasma flow.

1. INTRODUCTION

Transversely heated ions are a common feature of the Earth's magnetosphere. Since the early observations of such ions during the late seventies [e.g., *Whalen et al.*, 1978; *Klumpar*, 1979], a great deal of work has gone into understanding the generation and transport of such ions [e.g., *Chang*, 1986; *Klumpar*, 1986]. However, most treatments on the transport employ the test particle approach, in which a perpendicularly heated ion is transported under the action of the upward mirror force proportional to the gradients in the magnetic field. Only recently, time-dependent models have been employed to study the generation and transport processes and their effects on the ambient plasma [*Ganguli and Palmadesso*, 1987; *Brown et al.*, 1991; *Singh*, 1992]. The aspect of the plasma perturbations created by the transverse ion heating was emphasized by *Singh* [1992]. Among the noteworthy features of the plasma perturbations are the formation of density depletion and enhancement, and generation of parallel electric fields. For impulsive heating, an interesting feature of the parallel field is that it occurs in the form of a nearly unipolar upward pointing electric field pulse, which moves upward with a velocity of several tens of kilometers per second. However, a large-scale model dealing with distances of thousands of kilometers is limited in its temporal and spatial resolutions. On the other hand, electric fields seen in the auroral plasma [*Temerin et al.*, 1982] have spatial size of a few meters and corresponding time scale of about a few milliseconds. Therefore, in the previous work of *Singh* [1992], it was not clear at all how such an electric field pulse can be compared with weak double layers.

The purpose of this paper is to study the perturbations created by the transverse ion heating, using a small-scale particle-in-cell code having the capability of resolving distances of a few Debye lengths and time of a few milliseconds. The particle simulation reveals the same basic feature

of the plasma perturbations generated by the transverse ion heating as seen from the large-scale hydrodynamic study, namely, the formation of a density cavity topped by a density enhancement, and eventually, the evolution of the density perturbation into a reverse-forward shocks pair. The unipolar upward pointing electric field occurs near the forward shock. The maximum electric field in the pulse is a few millivolts per meter, and its spatial dimension is a few tens of meters. These features of the pulse, including its upward velocity of about 50 km/s, have striking resemblance with the weak double layer seen from satellite [*Temerin et al.*, 1982; *Boström et al.*, 1988].

Kinetic simulations show additional noteworthy features involving multistreaming of ions. Above the perturbations in the density, ions with relatively large energies stream upward, setting up an ion conic type of flow on top of the ambient polar wind. In the midst of the density depletion and the enhancement, two streams of up flowing ions appear, which eventually couple together through ion-ion instability. It is interesting to point out that if the grid size in the simulation is increased beyond a certain limit, the ion-ion instabilities are not seen. This implies an important limitation of large-scale models, in which the usage of large grid size eliminates the possibility of coupling the ion streams. Futhermore, the large grid size and the corresponding large time steps eliminate the process of steepening of a compressive density perturbation forming a shock, like the forward shock near the density enhancement.

The fast ions above the forward shock appear like "elevated" ion conics with a low cutoff energy, which increases with increasing distance from the heating region. Futhermore, the density of such conics decreases monotonically with the distance. This suggests that ion conics can be found far from the regions of strong density perturbations in the plasma, created by the heating process.

The rest of the paper is organized as follows. The simulation technique is described in section 2. Numerical results on the plasma perturbations are described in section 3. The paper is concluded in section 4.

2. Simulation Model

We use a particle-in-cell code to solve for the dynamics of ions flowing along a diverging flux tube (Figure 1). The electrons are assumed to obey the Boltzmann distribution, which in conjunction with the quasineutrality condition yields the electric field parallel to the magnetic field. As mentioned in the introduction, the flux tube simulated is artificial in the sense that magnetic field is reduced by a factor of 2 over a distance of about $s_{max} = 7.5$ km. This is done to hasten the transport of the transversely heated ions by the mirror force. The ion heating occurs over a limited region of space (Figure 1). Ions in this region are given a random impulse $\delta w_\perp$ in the perpendicular direction according to a Maxwellian probability density function given by [*Brown et al.*, 1991; *Puri*, 1966]

$$P(\delta w_\perp) = \frac{1}{\sqrt{\pi}\sigma} e^{-\delta w_\perp^2/\sigma^2}. \qquad (1)$$

The energy of the ions is given by

$$w_{\perp f} = w_{\perp i} + \delta w_{\perp} + 2\sqrt{w_{\perp i}|\delta w|}cos\phi \qquad (2)$$

where $w_{\perp i}$ and $w_{\perp f}$ are the perpendicular energies of the ions at the beginning and end of a time step, and ϕ is an angle between 0 and 2π randomly chosen from a uniform probability density function. The heating rate is related to σ according to $\sigma = 1.14\Delta t(\partial w_{\perp}/\partial t)$, where $w_{\perp} = 1/2mV_{\perp}{}^2$, m is the ion mass and $V_{\perp}$ is the perpendicular velocity.

The ion motion is advanced by solving the equation of motion

$$m\frac{d^2s}{dt^2} = qE_{\parallel} - \mu\frac{\partial B}{\partial s} \qquad (3)$$

where m and q are the mass and charge of an ion, $E_{\parallel}$ is the electric field, μ is the magnetic moment of the ion, and $\partial B/\partial s$ is the gradient in the magnetic field.

The parallel electric field, $E_{\parallel}$, is calculated by assuming that the plasma remains quasineutral, i.e., $n_e \simeq n_i$, where n_e and n_i are the electron and ion densities, respectively. Futhermore, electrons are assumed to be a massless isothermal fluid. The electron momentum equation gives

$$E_{\parallel} = -\frac{kT_e}{e}\frac{1}{n_e}\frac{\partial n_e}{\partial s} \qquad (4)$$

where k is the Boltzmann constant and T_e is the electron temperature.

As we will see later, the scale lengths in the plasma perturbations studied here are several tens of meters while the plasma Debye length is a few meters. Therefore the space charge effects are ignorable and quasineutrality is a good approximation. The assumption of electrons being massless eliminates the effects of velocity gradients in the flow. Since in the present calculations we assume that there is no field-aligned current and $n_e \simeq n_i$, it is implied that $V_e = V_i$, where V_e and V_i stand for electron and ion flow velocities, respectively. In the calculations presented here, we assume $T_e = 1$ eV, for which electron thermal velocity, $V_{te} \simeq 400$ km/s. In the perturbations discussed in this paper, the flow velocities V_e and $V_i \leq 15\ V_{ti}$, where V_{ti} is the ion thermal velocity, which is about 5.5 km/s. Therefore we find that $V_e^2 \simeq V_i^2 << V_{te}^2$. This ensures that the assumption of electrons being massless is justified. Futhermore, it also justifies the assumption of electrons being isothermal.

3. Numerical Results

3.1 Summary of Results From the Fluid Model

The origin of this paper lies in a previous paper [*Singh*, 1992], in which plasma perturbations created by transverse ion heating were studied, using a large-scale model based on fluid equations for the plasma. Since our goal in this paper is to examine how the results from a kinetic treatment of ions compare and contrast with the results from the fluid treatment, it is useful to briefly review the latter results. Figures 2*a* to 2*h* show the basic nature of the perturbations in density, flow velocity, parallel temperature, perpendicular temperature, and the parallel electric field when the heating occurs over 5s over a heating region of 210-km length at an altitude of 5500 km. The heating rate is 240 eV/s and

electron temperature is assumed to be 10 eV. Figures 2*a* to 2*h* show the evolution of the perturbation up to $t = t_4 = 2$ min. Note that $t_n = n \times 30$ s. We find that at an early time ($t \leq t_1$) the basic feature of the perturbation is the formation of a plasma cavity topped by a density enhancement (Figure 2*a*). At later times, the density perturbation evolves into a reverse-forward shock pair, as indicated by "R" and "F". The leading edge of the perturbation is the forward shock (F) and the trailing edge of the density enhancement is the reverse shock (R). The entire perturbation is seen moving upward. However, the trailing edge of the perturbation moves much slower than the leading edge (F), resulting in the creation of an extended cavity which expands upward. Figure 2*b* shows that the flow velocity is perturbed over the entire region of the density perturbation and it has the feature of a double sawtooth; the tooth near the forward shock is sharp, while near the reverse shock it is relatively shallow. When the heating continues for a longer time, the reverse shock also evolves into sharp jumps [*Singh*, 1992].

The temperature profile for $T_\parallel$ shows a cooling in the plasma cavity and an increase in the density enhancement between the reverse and forward shocks. The transverse heating yields a maximum perpendicular temperature of 100 eV at $t = t_1$ and the maximum temperature adiabatically decreases later on. The enhancement in $T_\perp$ is limited to altitudes below the forward shock. Later we show how this feature is appreciably modified when the ions are treated kinetically.

The electric field perturbations for the transverse heating are shown in Figures 2*e* to 2*h*. The most noteworthy feature of the electric field distribution shown in this figure is its evolution to predominantly unipolar upward pointing electric field near the leading edge of the density bump when $t \geq t_2 \approx 1$ min. This dominant electric field pulse propagates upward with a velocity of about 60 km/s, which is about twice the H^+ ion acoustic speed with 10-eV electrons. Such upward propagating electric field pulses appear quite similar to the predominantly unipolar electric fields observed in the auroral plasma [*Temerin et al.*, 1982]. However, the observed fields are generally interpreted as ion acoustic double layers which have scale length of a few tens of Debye lengths (~ 100 m). In contrast, in the hydrodynamic calculations we have a spatial resolution of 60 km and temporal resolution of 1s, which are, respectively, the intergrid spacing and the time step used in our calculations. In the following discussion, we present results from a kinetic treatment of ions with spatial and temporal resolutions capable of resolving ion dynamics at a time scale of ion-plasma period.

3.2 Results From a Small-Scale Kinetic Model

We first ran the simulation without any heating until a polar wind type of flow is set up in the artificial flux tube. For the parameters chosen here, this takes about 1200 ω_{pio}^{-1}, where ω_{pio} is the ion plasma frequency at s = 0, where normalized density is unity. When the flow is established, the heating is switched on over the spatial region $50 \leq s/\lambda_{di} \leq 250$. The heating rate $\partial W_\perp/\partial t$ is about $\omega_{pio} k T_0$, where k is the Boltzmann constant and T_0 is the ion temperature at the

boundary s = 0. The flux tube length is $S_{max} = 7500\lambda_{di}$. For the parameters chosen here the plasma density at the bottom of the flux tube is 20 cm^{-3} and temperature T_0 = 0.3 eV, giving ion Debye length $\lambda_{di} \approx 1$ m, $S_{max} = 7.5$ km and heating rate $(\partial W_\perp/\partial t)$ is 1800 eV/s. The heating is kept on over a time period of $\Delta t_h = 40\omega_{pio}^{-1} \approx 5$ ms.

3.3 Perturbation in Phase Space

The evolution of the heated ions is shown in Figures 3*a* and 3*b* which give the temporal evolution of phase-space in $S - V_\parallel$ and $S - V_\perp$ planes, respectively. At $\tilde{t} = 1400$, where $\tilde{t} = t\omega_{pio}$, heated ions are still relatively localized near the heating region. At later times they flow upward under the action of the mirror force leading to an increase in parallel velocity(energy) at the expense of the perpendicular velocity (energy). As the ions flow upward, the phase-space plots show that double streaming develops both near the top and bottom of the perturbation. The two streams at the top consist of transversely heated ions, which have gained considerable parallel energies under the action of the mirror force, and the ambient polar wind ions. The relative parallel velocity between these two ion populations is sufficiently high and therefore they do not show any sign of ion-ion interaction causing instability [*Gresillon and Doveil*, 1975].

In the bottom most part of the perturbation ions appear to be primarily accelerated in their parallel velocities, but above a certain height depending on time, another stream appears. The latter stream is relatively slower. In the regions where these streams overlap, there are vortices in the $S - V_\parallel$ plots. These vortices are the consequence of ion-ion instability, which we shall discuss later on. By the time $\tilde{t} \approx$ 2200, the major part of the perturbation in terms of transversely heated ions has almost exited from the top of the flux tube, but there are still perturbations persisting in $V_\parallel$ extending to much lower heights.

The distribution function of the ions in the perturbation region ($3750 \leq S/\lambda_{di}$ 7500) is shown for $\tilde{t} = 1800$ in Figure 4*a*, which gives the scatter plots of ions in $V_\perp - V_\parallel$ plane. Transverse acceleration of ions and associated parallel acceleration due to the mirror force is clearly seen. However, we also find some ions gaining only a parallel energy corresponding to the increase in parallel velocity up to $V_\parallel \approx 15V_{ti}$. This parallel acceleration is the consequence of the random nature of the ion heating; ions gain perpendicular energies at some stage of the heating and then lose a part of it at a later stage, after they have moved upward, and converted a part of the earlier gained energy into their parallel velocity component. However, the important feature of the random heating is the production of ion conics elevated in parallel energy. The elevation in parallel energy is more clearly seen if only the ions above the strong perturbation in the density, where double streaming occurs, are examined. This is shown in Figure 4*b* for ions with $S > 6000$ λ_d at $\tilde{t} = 1800$.

3.4 Perturbation in Average Flow Properties

We now compare the basic features of the plasma perturbations produced by the heating in the hydrodynamic

(Figures 2a to 2h) and kinetic models. For the latter model, the evolution of the perturbations in the bulk plasma parameters such as density, flow velocity, and effective parallel and perpendicular temperatures are shown in Figures 5*a* to 5*d*. It is important to point out that the comparison is not quantitative, only the basic features of the perturbations are compared here. As expected the localized heating creates a density cavity topped by a density enhancement. The entire perturbation rides on top of an upward expanding polar wind into a plasma cavity created by the heating. Unlike in the hydrodynamic model (see Figure 2a), the leading portion of the density enhancement has a perturbation extending to relatively large distances. The extended perturbation is the consequence of the fast ions running ahead of the major perturbation in the density (see Figure 3). However, like in the hydrodynamic model [*Singh*, 1992], there is a sharp gradient near the leading edge of the density enhancement and it occurs where the $S - V_{\|}$ phase-space plot forks into two distinct branches consisting of the ambient polar wind and the transversely accelerated ions as indicated by downward arrows in Figure 3a. Below the fork, the hydrodynamic predictions are expected to be true and above it, double streams occur with large relative velocities, and the hydrodynamic model fails. The sharp gradient in the density profile is the forward shock found from a hydrodynamic model [*Singh*, 1992]. The shock separates the fast streaming ions above it from the mixed, and relatively warm just below it.

The velocity profiles in Figure 5*b* show that at $\tilde{t} = 1400$, the perturbation is beginning to develop a double-sawtooth structure and it is fully developed at $\tilde{t} = 1600$. The lower sawtooth in the perturbation occurs near the trailing edge of the density enhancements, where downward electric fields occur and retard the upward flow of transversely heated ions. This retardation of ions produces the doublestream (Figure 3*a*) feature in the reverse shock region. The hydrodynamic model fails to handle such a double-streaming. The top sawtooth occurs near the leading edge of the density enhancements, the forward shock. However, due to the fast ions running ahead of the forward shock, the slope of the leading tooth is considerably reduced. For later times shown in Figure 5*b*, the upper sawtooth has exited from the top and only the lower sawtooth can be seen.

It is worth noting that above the forking point in $S - V_{\|}$ space (Figure 3*a*), where double streams occur, the average flow velocity does not give the true velocity of the transversely heated ions because the relatively dense cold stream (polar wind) weighs down the flow velocity. As mentioned earlier, this region is not treated properly by a hydrodynamic model.

In Figure 5*c*, we show the evolution of the effective parallel temperature calculated from the equation

$$T_{eff}(l\Delta S) = \sum_{j=1}^{N} m_i (V_j - V)^2 / N \qquad (5)$$

where N is the number of particles in a cell of length $\Delta s = 75\lambda_{di}$, and $l\Delta s$ is the distance from s = 0 with l as an integer.

The parallel temperature profiles show a cooling of ions in

the lowest part of the perturbation. Cooling occurs as the polar wind expands into the plasma cavity created by the transverse ion heating. Such a cooling is also predicted by the hydrodynamic model (Figure 2*c*). However, the effective temperature is seen to be elevated considerably beyond the forking point in the phase-space plots in $S - V_{\|}$ plane (Figure 3*a*). This is simply because above the forking point there are double streams and the concept of a single temperature for the entire ion population is not valid.

The evolution of the effective perpendicular temperature is shown in Figure 5*d*. In this case also, it is worth mentioning that above the forking point in $S - V_{\|}$ phase-space, there are two streams and the effective temperature does not give the true picture of the heated ions because the relatively dense cold ion stream (polar wind) weighs down the temperature significantly. It is important to point out that the heated ions above the the forking point in the $S - V_{\|}$ plots (Figure 3*a*) are completely lost in a hydrodynamic model, and these are the ions which appear as ion conics (Figure 4*a* and 4*b*). There are heated ions even below the forking point, but they represent an ion population having undergone a bulk heating, as a consequence of the merger of the polar wind and transversely heated ions. The hydrodynamic model can properly handle this portion of the perturbation.

3.5 Parallel Electric Field Generation

Figure 6 shows the evolution of the parallel electric field generated by the transverse ion heating. The plot at $\tilde{t} = 1200$ shows essentially the noise in the simulation system just before the heating. At $\tilde{t} = 1400$, we notice the development of a triplet in the electric field perturbation, consisting of upward (positive) fields in its bottom most part, downward (negative) fields in the middle, and a relatively localized solitary pulse with upward fields near its top. As the composite perturbation evolves, the solitary electric field pulse moves upward with a nearly constant speed; the propagation of the pulse is indicated by the slant line giving the trajectory of the peak of the pulse in *s-t* plane. The trajectory is obtained by projecting the peak point on the horizontal axis and joining the projection points in the panels for $\tilde{t} = 1600$, 1800 and 2000 in Figure 6. The slope of this line gives the propagation speed to be about $8.4V_{ti}$, which is about 46 km/s for the parameters chosen for the run. The pulse width of the electric field is about 200 m. The maximum field strength is about $6 \times 10^{-3} E_0 \approx 2$ mV. However, it is worth mentioning that the field strength depends on the electron temperature as given by equation (4). For higher electron temperatures, a higher field strength is expected. For example, if T_e was chosen to be 10 eV, fields up to 20 mV/m are expected, and for $T_e = 100$ eV, the fields scale to be as high as 200 mV/m. Even the shock processes may enhance T_e and hence the electric field. [*Forslund and Shonk*, 1970]. The electron temperature enhancement occurs when the electrons are trapped in the potential well created by the density enhancement. However, in the present calculations we have assumed electrons to remain isothermal and hence such effects are not included.

Figure 6 shows that, in the wake region of the solitary electric field pulse, oscillating fields develop. Such fields are

clearly seen for $\tilde{t} \geq 1600$ and they are well developed at $\tilde{t} \geq 2000$. The amplitude of the wave is seen to increase to $8 \times 10^{-3} E_0 \approx 2.5$ mV/m. The oscillating fields are associated with vortices in $S - V_{\parallel}$ phase space (Figure 3a). The vortices can be barely seen from Figure 3. Therefore, we have replotted them on an expanded scale in Figure 7 for $\tilde{t}$ = 2200; the vortex size ranges between 100 to 250 λ_{di}, which corresponds to the range in the wavelength of the spatial oscillations in the parallel fields. The vortices occur over $3750 \leq s/\lambda_{di} < 5625$, which is the spatial region in which the oscillating fields occur at this time (see Figure 6*e*).

The ion-ion instability occurs when the relative velocity (V_{rel}) between the streams is limited to $V_{rel} \leq 2C_s$ [e.g., *Gresillon and Doveil*, 1975; *Singh*, 1978], where C_s is the ion-acoustic speed. In our calculation, $T_e = 3.3T_0$, for which $C_s \simeq 2V_{ti}$, where V_{ti} is the ion thermal velocity given by $(kT_0/m)^{1/2}$. Thus the coupling is expected to occur when $V_{rel} \leq 4V_{ti}$. The space-phase plots (Figure 3*a*) show that for the double streaming in the reverse shock region, this velocity condition is well satisfied. On the other hand, for the double streaming above the forward shock, the two streams are generally too fast to drive the ion-ion interaction. However, for such fast streams ion-electron interaction may lead to instabilities, which occur when the negative energy (slow) mode of an ion beam is damped by the Landau damping caused by the thermal electron population [*Singh*, 1978]. In the present model, electrons are assumed to obey the Boltzmann Law, so this kinetic instability is suppressed from the model.

3.6 Numerics Versus Physics

Plasma problems in space involve a wide variety of scale lengths, ranging from plasma Debye length to the geophysical distances. This makes it impossible to develop self-consistent models including both small- and large-scale processes. Recently, large-scale semikinetic models have been developed to study the polar wind [*Wilson et al.* 1990; *Brown et al.*, 1991; *Ho et al.*, 1992] and the plasmaspheric refilling [*Lin et al.*, 1992; *Wilson et al.*, 1992]. These models employ a particle code in which the number of particles is limited to about 10^5, filling a flux tube of length up to several earth radii. Thus the models have, on the average, about 1 particle per kilometer. In these models, electric fields are calculated from the ion density, which is obtained by the number of particles in numerical cells and their volumes. In order to have reasonable statistics, the cell size is typically several tens of kilometers. Due to these reasons, the large-scale kinetic models suppress the microprocesses, even though the codes treat ions kinetically.

In order to demonstrate the above points on how the numerics suppress the physical processes, we repeated the calculations presented earlier with different grid sizes for calculating the electric fields. The evolution of $S - V_{\parallel}$ phase space for different grid sizes is shown in Figures 8*a* to 8*f*; $\Delta s = 5\lambda_d$ for Figures 8*a* and 8*b*; $\Delta s = 20\lambda_d$ for Figures 8*c* and 8*d*; and $\Delta s = 100\lambda_d$ for Figures 8*e* and 8*f*. The left- and right-hand columns of Figure 8 show different stages of the evolution of the ion-ion instability which occur in the perturbations. For $\Delta s = 5\lambda_d$ (Figure 8*a* and 8*b*) the instability,

manifested by the vortices, is much more fine grained than that for $\Delta s = 20\lambda_d$ (Figures 8*c* and 8*d*), for which the vortex formation is quite clear, especially at $\tilde{t} = 2200$. When Δs is increased to $100\lambda_d$ (Figures 8*e* and 8*f*), the instability does not occur at $\tilde{t} = 1800$, and at $\tilde{t} = 2200$ the vortex structure tends to appear, but is not strong enough to fully couple the two ion streams. When Δs is further increased, the instability nearly disappears, even though the ion streams have nearly the same bulk properties, such as the flow velocity, density and temperature.

In order to understand the above feature of ion-ion instability and its numerical realization, we discuss here briefly its linear properties. The ion-ion instability is limited to relatively long wavelengths given by $\lambda \geq 2\pi V_{rel}/\omega_{pi}$, where V_{rel} and ω_{pi} are, respectively, the local relative velocity between the streams and the ion plasma frequency. In the present situation the relative velocity is about $4V_{ti}$ and $\omega_{pi} \approx 0.4\omega_{pio}$ (corresponding to a local density of 0.2 inside the cavity), giving $\lambda \geq 80\lambda_{di}$. However, the waves are strongly excited near the lower limit on the wave lengths [see *Baker*, 1973]. Therefore, when $\Delta s = 5\lambda_d$, the growing waves are properly described by the numerics because there are several grid spacings in a wavelength. In Figures 8*a* and 8*b*, the size of the vortices is about $100\lambda_{di}$. When Δs is increased to $20\lambda_{di}$, the relatively short wavelength waves are eliminated numerically and those left have a relatively long wavelength. In Figures 8*c* and 8*d*, the vortices are separated by about $200\lambda_d$. When Δs is increased to $100\lambda_d$, the instability is almost entirely eliminated by the numerics. However, Figure 8*f* does show a relatively weak vortex structure, as expected from the fact that the long wavelength waves, not unaffected by the large grid size, have relatively small growth rates [*Baker*, 1973].

The above discussion shows that in order to properly model the ion waves associated with ion streams in space, a sufficiently small resolution depending on the ion parallel energy and plasma density, is needed. For typical energies and densities in the auroral plasma at relatively high altitudes, the resolution required is ≤ 1 km. Therefore large-scale models even though they may be kinetic, fail to treat the microprocesses, and results from them under the conditions of counterstreaming and double streaming must be treated with caution.

4. Conclusion and Discussion

The main aim of this paper is to study the variety of plasma processes which can be driven by localized transverse ion heating in a diverging flux tube. Although we have simulated here an artificial flux tube, the main motivation for this study is the transverse ion heating occurring in the Earth's magnetosphere, producing the well-known phenomenon of ion conics. The self-consistent generation and transport of ion conics, including the driven microprocesses, are almost impossible to model theoretically because of the range of scale lengths involved in space plasmas. Therefore, in order to develop a feel for the possible processes we have adopted an artificial diverging flux tube, in which effects of the transverse ion heating on the plasma are simulated. As described in the previous section, the results from this initial

study are interesting because they show that the transverse ion heating does not just produce ion conics, it also drives a host of plasma processes, some of which are revealed here by the simulation. Among the important processes revealed are the formation and dynamics of plasma density perturbations, generation of parallel electric fields, multistreaming of ions, and ion-ion interactions generating oscillating field-aligned electric fields.

The generation of parallel electric fields by transverse ion heating is a novel concept. For heating localized to a few km, the electric field pulse near the forward shock had upward fields, it moves upward, and has the spatial and temporal features of weak double layers. Can such fields account for weak double layers observed in space [*Temerin et al.*, 1982; *Block et al.*, 1987; *Boström et al.*, 1988]? At this time this is an open question and its answer lies in a rigorous scrutiny of the theoretical results in view of the observed features of the fields in space. This has not been done here.

The above feature of the plasma perturbations driven by the transverse ion heating was previously predicted from a hydrodynamic model for the polar wind plasma flow [*Singh*, 1992]. However, in that study the spatial and temporal features were too coarse to predict the fine temporal and spatial features of the parallel electric fields obtained here. Figure 6 shows that the spatial size of the electric field pulse is $\sim$ 100 m; it moves with a velocity of about 50 km/s and the corresponding time scale of the pulse is 2 ms.

The double streaming of ions produced by transverse ion heating is noteworthy. The double streaming occurring in the midst of the density perturbation is the consequence of the upward acceleration of some ions by the mirror force while some ions are being retarded downward by the downward electric field in the reverse shock region. This multistreaming produces ion waves generating oscillating parallel electric fields. The role of such fields in electron heating is mentionable. However, the present simulation model does not allow it because electrons are assumed to obey the Boltzmann law.

The double streaming of ions above the forward shock is produced by the relatively slow polar wind ions being overtaken by the fast ions produced by transverse ion heating. The latter ions have the feature of "elevated" ion conics [*Temerin*, 1986; *Horwitz*, 1986; *Hultqvist et al.*, 1988]. The double streams on the top of the perturbation do not excite ion-ion instability because their relative velocity is too fast. However, the presence of relatively warm electrons may change this by increasing the ion-acoustic speed.

In the present model, electron dynamics is highly simplified through the assumption that the electrons obey the Boltzmann law. If this assumption is relaxed, electrons are likely to be energized by the parallel fields, especially by the oscillatory fields driven by ion-ion instability. One of the puzzling observations in space is the simultaneous measurement of elevated ion conics and field-aligned electrons with comparable energies [*Hultqvist et al.*, 1988]. These particle populations are observed in conjunction with electrostatic noise in the frequency range from zero to 300 Hz. The simulations presented here show how a localized heating can generate the elevated ion conics and the field-aligned electric

fields which are capable of heating electrons in the parallel direction. If electron dynamics is included in the model, possibly other wave modes through ion-electron interaction can be driven. Simulations with full electron dynamics are needed to see if the puzzling observations by *Hultqvist et al.* [1988] can be explained by localized ion heating and the processes driven by it.

We have quantitatively demonstrated here how large-scale hydrodynamic and kinetic codes suppress the small-scale features of plasma flow because of their inherent coarseness. Small-scale simulations which keep the essential features of the problems in space and, at the same time, have sufficient spatial and temporal resolutions, can elucidate the important microprocesses which effectively control the properties of the plasma flow. This paper presents an initial attempt towards the goal of understanding the generation and transport of ion conics and associated plasma processes.

Results presented in this paper are based on assumptions such as (1) plasma being quasineutral, (2) electrons are a massless isothermal fluid, and (3) the simulation is one-dimensional. We already discussed that for the parameters chosen in the present simulations the assumptions 1 and 2 are justified. However, for situations involving other set of parameters, the results presented here can be only qualitatively correct. For example, if the heating produces a large flow velocity approaching the electron thermal velocity, the assumption of electrons being isothermal is not justified. This situation requires a more rigorous treatment of the electron dynamics. We are currently investigating such situations and results will be reported later.

The assumption of one-dimensional simulation model limits the treatment of the ion-ion instability. In a multidimensional situation, ion beams with relative velocities $V_{rel} > 2C_s$ can couple together through ion-ion instability [see *Karimabadi et al.*, 1991]. The coupling occurs through waves propagating at oblique angles with respect to the flow direction. The fast ions above the forward shock can participate in such instability processes. But the present simulation model is limited due to its dimensionality.

It is worth mentioning here that the hydrodynamic models have been used to study the transverse ion heating and their transport [*Ganguli and Palmodesso*, 1987; *Singh*, 1992]. The qualitative comparison of the results from the small-scale kinetic simulation and the large-scale hydrodynamic model shows that the latter model can not handle the phenomenon of ion conics and its transport; the temperatures and the flow velocity of the ion conics are grossly misrepresented. This is true despite the fact that the hydrodynamic models are quite sophisticated based on 16-moment approximation [*Barakat and Schunk*, 1982]. The major problem lies in handling the multistreaming consisting of the ion conics and the ambient plasma. Large-scale kinetic models [*Wilson et al.*, 1990; *Brown et al.*, 1991] do allow for multistreaming, but the problem lies in the coarse resolution and the consequent suppression of microprocesses which can critically affect the flow behavior. A rigorous treatment of the transport of ion conics including its interaction with the ambient plasma remains a challenge.

Acknowledgments. This work was supported by the Grant NAGW-2903 from NASA Headquarters to the University of Alabama in Huntsville.

The Editor thanks D. Winske and T. Onsager for their assistance in evaluating this paper.

REFERENCES

Baker, D. R., Nonlinear development of the two ion beam instability, *Phys. Fluids, 16*, 1730, 1973.

Barakat, A. R., and R. W. Schunk, Transport equations for multicomponent anisotropic space plasmas: A review, *Plasma phys., 24*, 389, 1982.

Block, L. P., C. G. Fälthammar, O. A. Lindqvist, G. T. Marklund, F. S. Moser, and A. Pedersen, Electric field measurement on Viking: First results, *Geophys. Res. Lett., 14*, 435, 1987.

Boström, R., G. Gustafsson, B. Holback, G. Holgren, H. Koskinen, and P. Kintner, Characteristics of solitary waves and weak double layers in the magnetospheric plasma, *Phys. Rev. Lett., 61*, 82, 1988.

Brown, D. G., G. R. Wilson, J. L. Horwitz, and D. L. Gallagher, Self-consistent production of ion conics on return current region auroral field lines: A time-dependent, semikinetic model, *Geophys. Res. Lett. 18*, 1841, 1991.

Chang, T. (Ed.), Ion Acceleration in the Magnetosphere and Ionosphere, Geophys. Monogr. Ser., vol. 38, AGU, Washington, D. C., 1986.

Forslund, D. W., and C. R. Shonk, Formation of electrostatic Collisionless Shocks, *Phys. Rev. Lett, 25*, 1699, 1970.

Ganguli, S. B., and P. J. Palmadesso, Plasma Transport in the Auroral Current Region, J. *Geophys. Res., 92*, 8673, 1987.

Gresillon, D., and F. Doveil, Normal modes in the ion-beam-plasma system, *Phys. Rev. Lett., 34*, 77, 1975.

Ho, C. W., J. L. Horwitz, N. Singh, T. E. Moore and G. R. Wilson, Effects of magnetospheric electrons on polar plasma outflow: A semi-kinetic model, *J. Geophys. Res., 97*, 8425, 1992.

Horwitz, J. L. Velocity filter mechanism for ion bowl distributions (Bimodal Conics), *J. Geophys. Res. 91*, 4513, 1986.

Hulqvist, B., On the acceleration of electrons and positive ions in the same direction along magnetic field lines by parallel fields, *J. Geophys. Res., 93*, 9777, 1988.

Karimabadi, H., N. Omidi, and K. B. Quest, Two-Dimensional Simulations of the ion-ion acoustic instability and electrostatic shocks, *Geophys. Res. Lett., 18*, 1813, 1991.

Klumpar, D. M., Transversely accelerated ions: An ionospheric source of hot magnetospheric ions, *J. Geophys. Res., 84*, 4229, 1979.

Klumpar, D. M. A digest and comprehensive bibliography on transverse auroral ion acceleration in *Ion Acceleration in the Magnetosphere and Ionosphere, Geophys. Monogr. Ser.*, vol. 38, edited by T. Chang, p. 389, AGU, Washington, D. C., 1986

Lin, J., J. L. Horwitz, G. R. Wilson, C. W. Ho, and D. G. Brown, A semikinetic model for early state plasmaspheric refilling, 2, Effects of wave-particle interactions, *J. Geophys. Res. 97*, 1121, 1992.

Puri, S., Plasma heating and diffusion in stochastic fields, *Phys. Fluids, 9*, 2043, 1966.

Singh, N., The ion-electron instability of ion-beam-plasma systems, *Phys. Lett., 67A*, 372, 1978.

Singh, N., Plasma perturbations created by transverse ion heating events in the magnetosphere, *J. Geophys. Res., 97*, 4235, 1992.

Temerin, M., Evidence of a large bulk ion conic heating region, *Geophys. Res. Lett., 13*, 1059, 1986.

Temerin, M., K. Cerny, W. Lottko, and F. S. Mozer, Observation of double layers and solitary waves in the auroral plasma, *Phys. Res. Lett.*, *48*, 1175, 1982.

Whalen, B. A., W. Bernstein, and P. W. Daly, Low altitude acceleration of ionospheric ions, *Geophys. Res. Lett.*, *5*, 55, 1978.

Wilson, G. R., C. W. Ho, J. L. Horwitz, N. Singh, and T. E. More, A new kinetic model for time-dependent polar plasma outflow: Initial results, *Geophys. Res Lett.*, *17*, 263, 1990.

Wilson, G. R., J. L. Horwitz, and J. Lin, A semi-kinetic model for early-stage plasmasphere refilling, 1, Effects of Coulomb collisions, *J. Geophys. Res.*, *97*, 1109, 1992.

C. B. Chan and N. Singh, Department of Electrical and Computer Engineering, University of Alabama in Huntsville, AL 35899.

(Received August 19, 1992;
revised October 19, 1992;
accepted November 23, 1992.)

---

paper number 92JA02789.
0148-0227/93/92JA-02789 $05.00

Singh and Chan: Plasma Processes Driven By Transverse Ion Heating
Singh and Chan: Plasma Processes Driven By Transverse Ion Heating
Singh and Chan: Plasma Processes Driven By Transverse Ion Heating
Singh and Chan: Plasma Processes Driven By Transverse Ion Heating
Singh and Chan: Plasma Processes Driven By Transverse Ion Heating
Singh and Chan: Plasma Processes Driven By Transverse Ion Heating
Singh and Chan: Plasma Processes Driven By Transverse Ion Heating
Singh and Chan: Plasma Processes Driven By Transverse Ion Heating
Singh and Chan: Plasma Processes Driven By Transverse Ion Heating
Singh and Chan: Plasma Processes Driven By Transverse Ion Heating
Singh and Chan: Plasma Processes Driven By Transverse Ion Heating
Singh and Chan: Plasma Processes Driven By Transverse Ion Heating
Singh and Chan: Plasma Processes Driven By Transverse Ion Heating
Singh and Chan: Plasma Processes Driven By Transverse Ion Heating
Singh and Chan: Plasma Processes Driven By Transverse Ion Heating
Singh and Chan: Plasma Processes Driven By Transverse Ion Heating
Singh and Chan: Plasma Processes Driven By Transverse Ion Heating
Singh and Chan: Plasma Processes Driven By Transverse Ion Heating
Singh and Chan: Plasma Processes Driven By Transverse Ion Heating
Singh and Chan: Plasma Processes Driven By Transverse Ion Heating

Singh and Chan: Plasma Processes Driven By Transverse Ion Heating

Singh and Chan: Plasma Processes Driven By Transverse Ion Heating

FIGURE CAPTIONS

Fig. 1. Geometry of the simulated flux tube. $N_0(20\ cm^{-3})$ and $T_0(0.3\ \text{eV})$ are the boundary values of plasma density and ion temperature.

Fig. 2. Plasma perturbations in response to an impulsive heating both in time and space ($\Delta t_h = 5$ s, $\Delta s_h = 60$ km). Electron temperature $T_e = 10$ eV. (a) to (d) The evolutions of $n(s)$, $v(s)$, $T_{\|}(s)$ and $T_{\perp}(s)$, respectively. (e) to (h) The evolution of the electric fields distribution.

Fig. 3a. Phase-space plots in $S - V_{\|}$ plane.

Fig. 3b. Phase-space plots in $S - V_{\perp}$ plane.

Fig. 4. Distribution of heated ions in $V_{\perp} - V_{\|}$ plane for (a) entire perturbation ($3700 \leq s/\lambda_{di} \geq 7500$) and ($b$) above the forking point ($s > 6000\lambda_{di}$) at $\tilde{t} = 1800$.

Fig. 5a. Perturbation in plasma velocity.

Fig. 5b. Perturbation in flow velocity.

Fig. 5c. Perturbation in parallel temperature.

Fig. 5d. Perturbation in perpendicular temperature.

Fig. 6. Evolution of the parallel electric fields; different panels show electric field profiles at the times indicated in the panels.

Fig. 7. $S - V_{\|}$ plot at $\tilde{t} = 2200$, showing the vortices on an expanded scale.

Fig. 8. Composition of $S - V_{\|}$ plots for different values of the spatial resolution: (a) $\Delta s = 5\lambda_{di}$, (b) $\Delta s = 20\lambda_{di}$, ($c$) $\Delta s = 100\lambda_{di}$.

FIGURE CAPTIONS

Fig. 1. Geometry of the simulated flux tube. $N_0(20\ cm^{-3})$ and $T_0(0.3\ \text{eV})$ are the boundary values of plasma density and ion temperature.

Fig. 2. Plasma perturbations in response to an impulsive heating both in time and space ($\Delta t_h = 5$ s, $\Delta s_h = 60$ km). Electron temperature $T_e = 10$ eV. (a) to (d) The evolutions of $n(s)$, $v(s)$, $T_{\|}(s)$ and $T_{\perp}(s)$, respectively. (e) to (h) The evolution of the electric fields distribution.

Fig. 3a. Phase-space plots in $S - V_{\|}$ plane.

Fig. 3b. Phase-space plots in $S - V_{\perp}$ plane.

Fig. 4. Distribution of heated ions in $V_\perp - V_\parallel$ plane for (a) entire perturbation ($3700 \leq s/\lambda_{di} \geq 7500$) and (b) above the forking point ($s > 6000\lambda_{di}$) at $\tilde{t} = 1800$.

Fig. 5a. Perturbation in plasma velocity.

Fig. 5b. Perturbation in flow velocity.

Fig. 5c. Perturbation in parallel temperature.

Fig. 5d. Perturbation in perpendicular temperature.

Fig. 6. Evolution of the parallel electric fields; different panels show electric field profiles at the times indicated in the panels.

Fig. 7. $S - V_\parallel$ plot at $\tilde{t} = 2200$, showing the vortices on an expanded scale.

Fig. 8. Composition of $S - V_\parallel$ plots for different values of the spatial resolution: (a) $\Delta s = 5\lambda_{di}$, (b) $\Delta s = 20\lambda_{di}$, (c) $\Delta s = 100\lambda_{di}$.

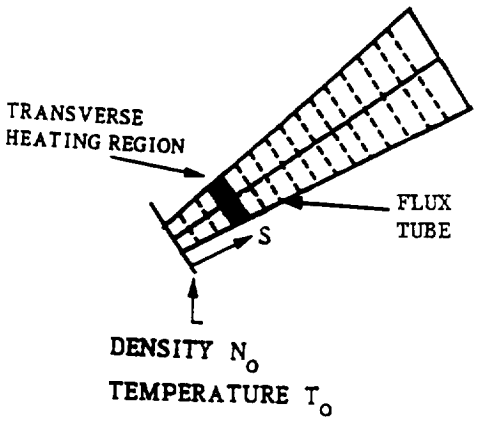
TRANSVERSE
HEATING REGION
FLUX
TUBE
S
DENSITY N_o
TEMPERATURE T_o

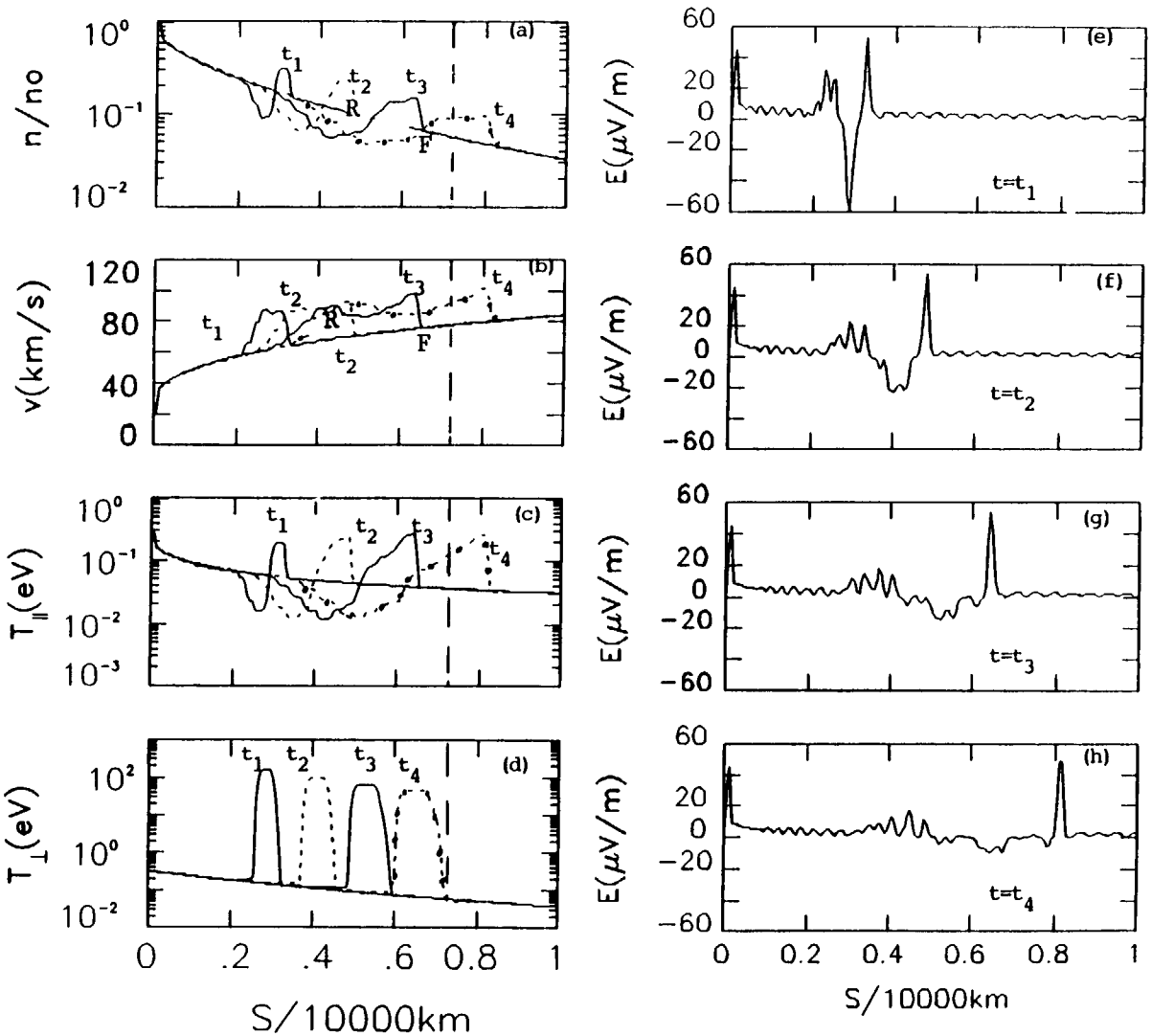
n/no
v(km/s)
T∥(eV)
T⊥(eV)
E(μV/m)
(a)
(b)
(c)
(d)
(e)
(f)
(g)
(h)
t1
t2
t3
t4
R
F
t=t1
t=t2
t=t3
t=t4
S/10000km

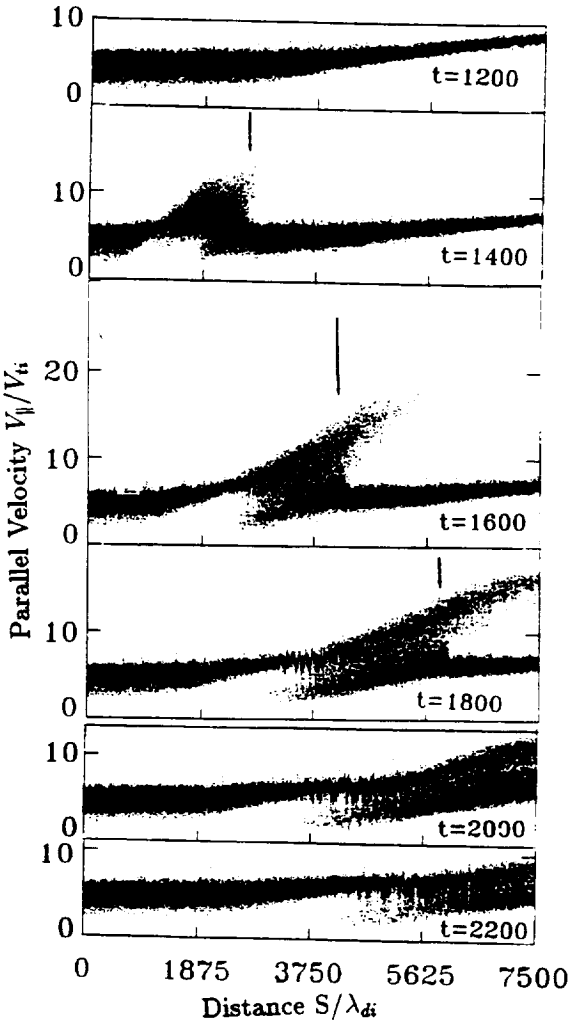
10
0
t=1200
10
0
t=1400
20
10
0
t=1600
10
0
t=1800
10
0
t=2000
10
0
t=2200
Parallel Velocity $V_{\parallel}/V_{ti}$
0
1875
3750
5625
7500
Distance S/λ_{di}

Fig. 3a

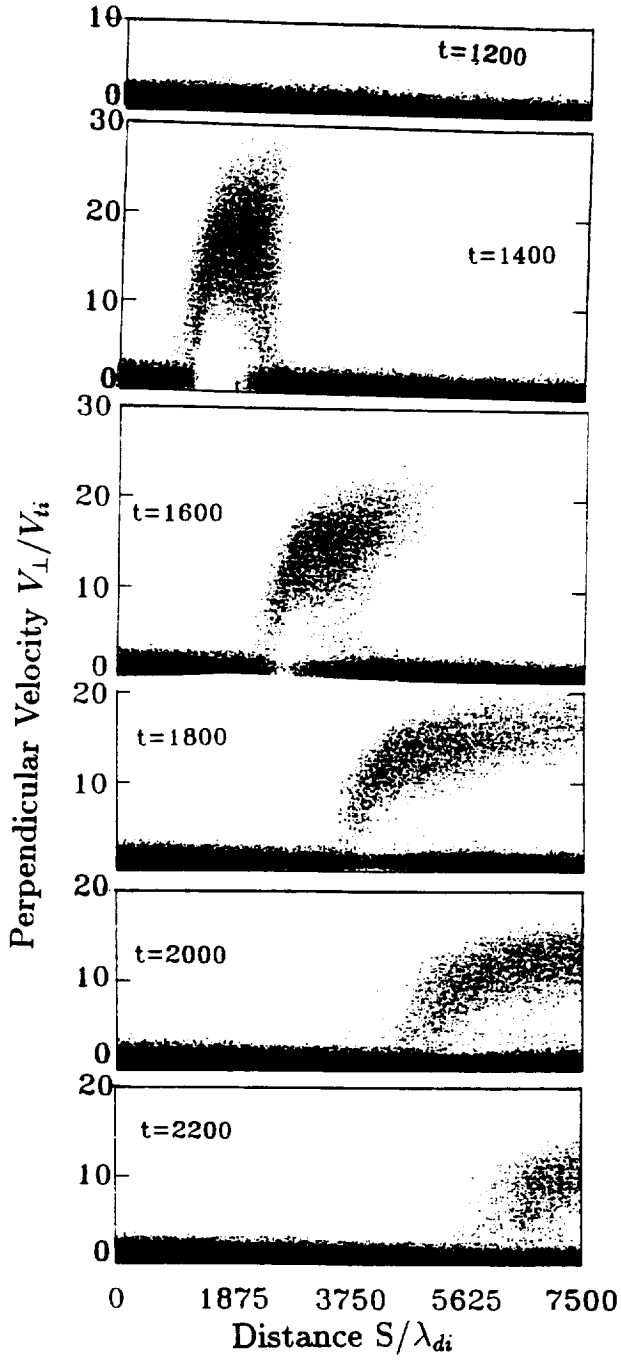
t=1200
t=1400
t=1600
t=1800
t=2000
t=2200
Perpendicular Velocity $V_\perp/V_{ti}$
0
1875
3750
5625
7500
Distance S/λ_{di}

Fig. 3b

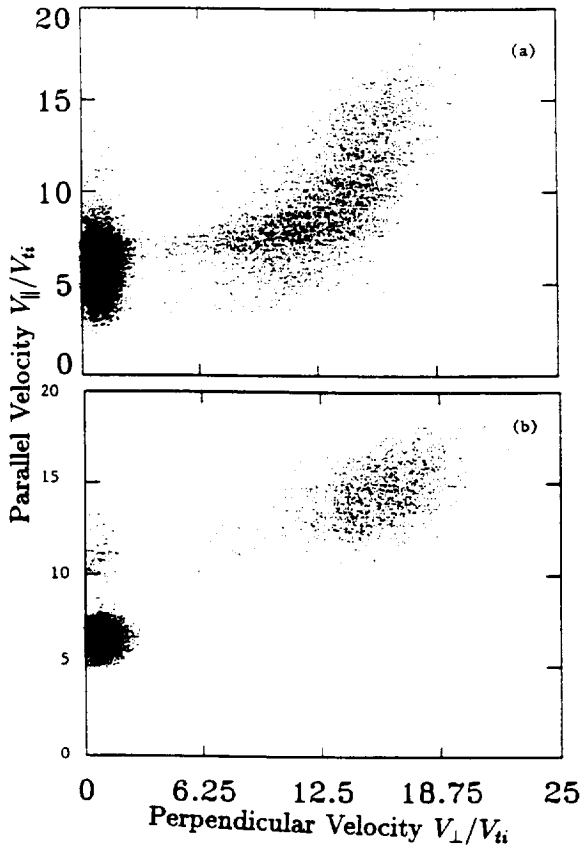
20
15
10
5
0
(a)
20
15
10
5
0
(b)
Parallel Velocity $V_{\parallel}/V_{ti}$
0
6.25
12.5
18.75
25
Perpendicular Velocity $V_{\perp}/V_{ti}$

Fig. 4

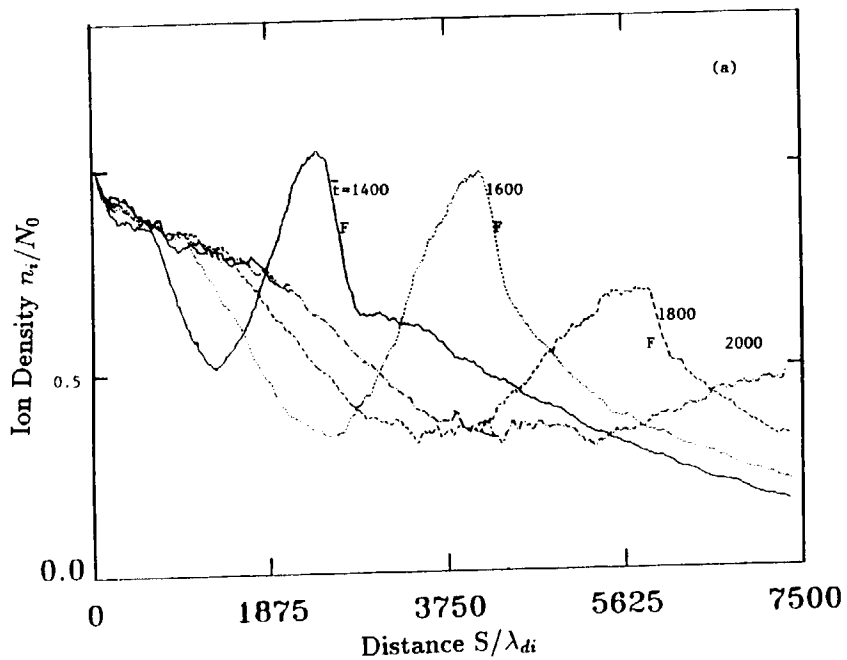
(a)
t=1400
1600
1800
2000
F
F
F
Ion Density n_i/N_0
0.5
0.0
0
1875
3750
5625
7500
Distance S/λ_{di}

Fig 5a

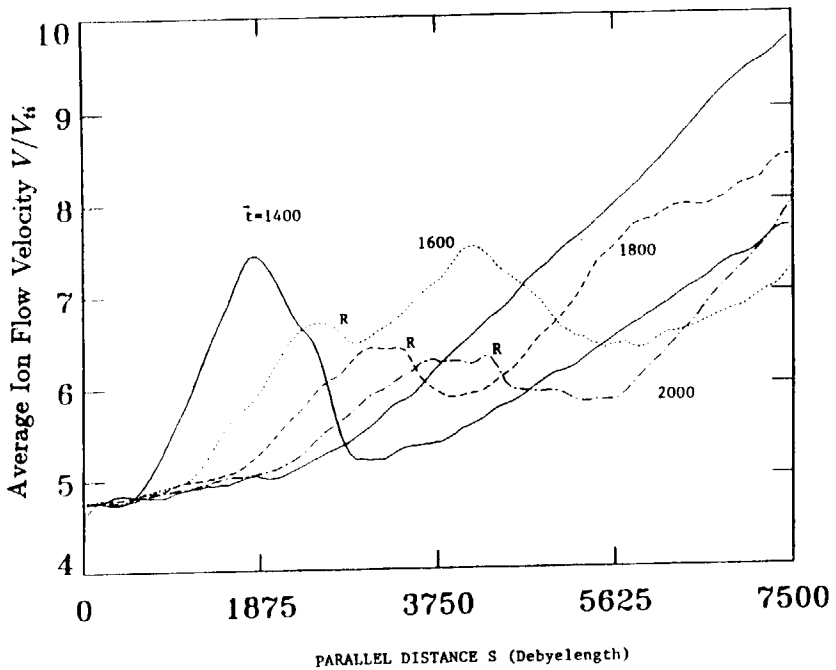
Average Ion Flow Velocity V/V_i
10
9
8
7
6
5
4
0
1875
3750
5625
7500
$\tilde{t}$=1400
1600
1800
2000
R
R
R
PARALLEL DISTANCE S (Debyelength)

Fig. 5b

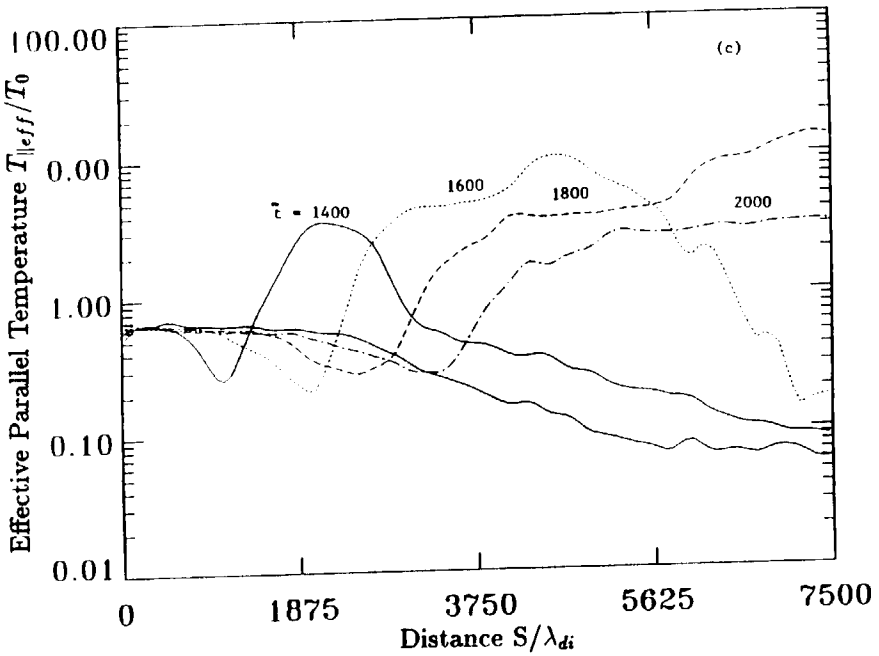
(c)
100.00
0.00
1.00
0.10
0.01
Effective Parallel Temperature $T_{\parallel eff}/T_0$
$\tilde{t}$ = 1400
1600
1800
2000
0
1875
3750
5625
7500
Distance S/λ_{di}

Fig. 5c

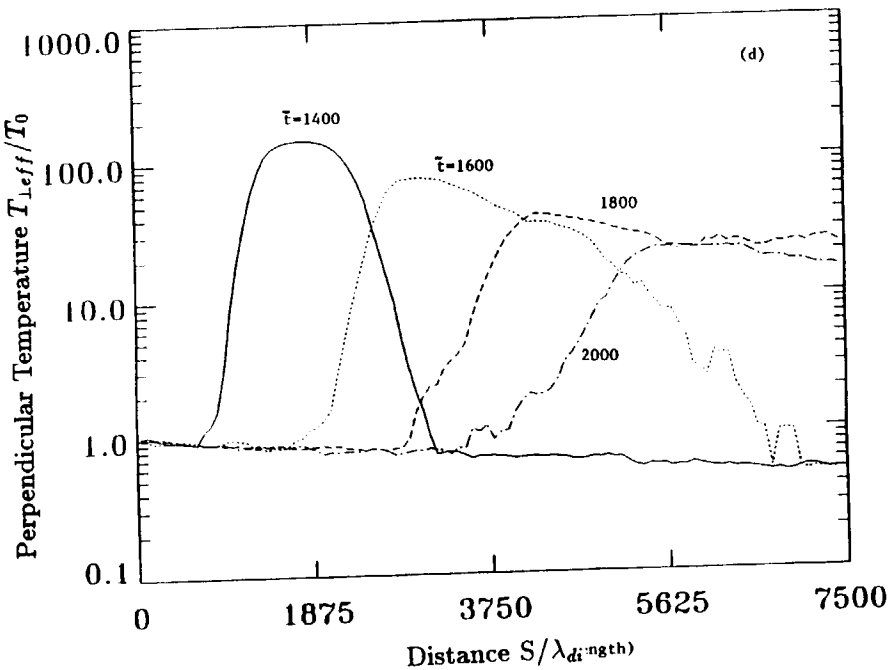
(d)
1000.0
100.0
10.0
1.0
0.1
Perpendicular Temperature $T_{\perp eff}/T_0$
$\bar{t}$=1400
$\bar{t}$=1600
1800
2000
0
1875
3750
5625
7500
Distance S/λ_{di}ngth)

Fig 5d

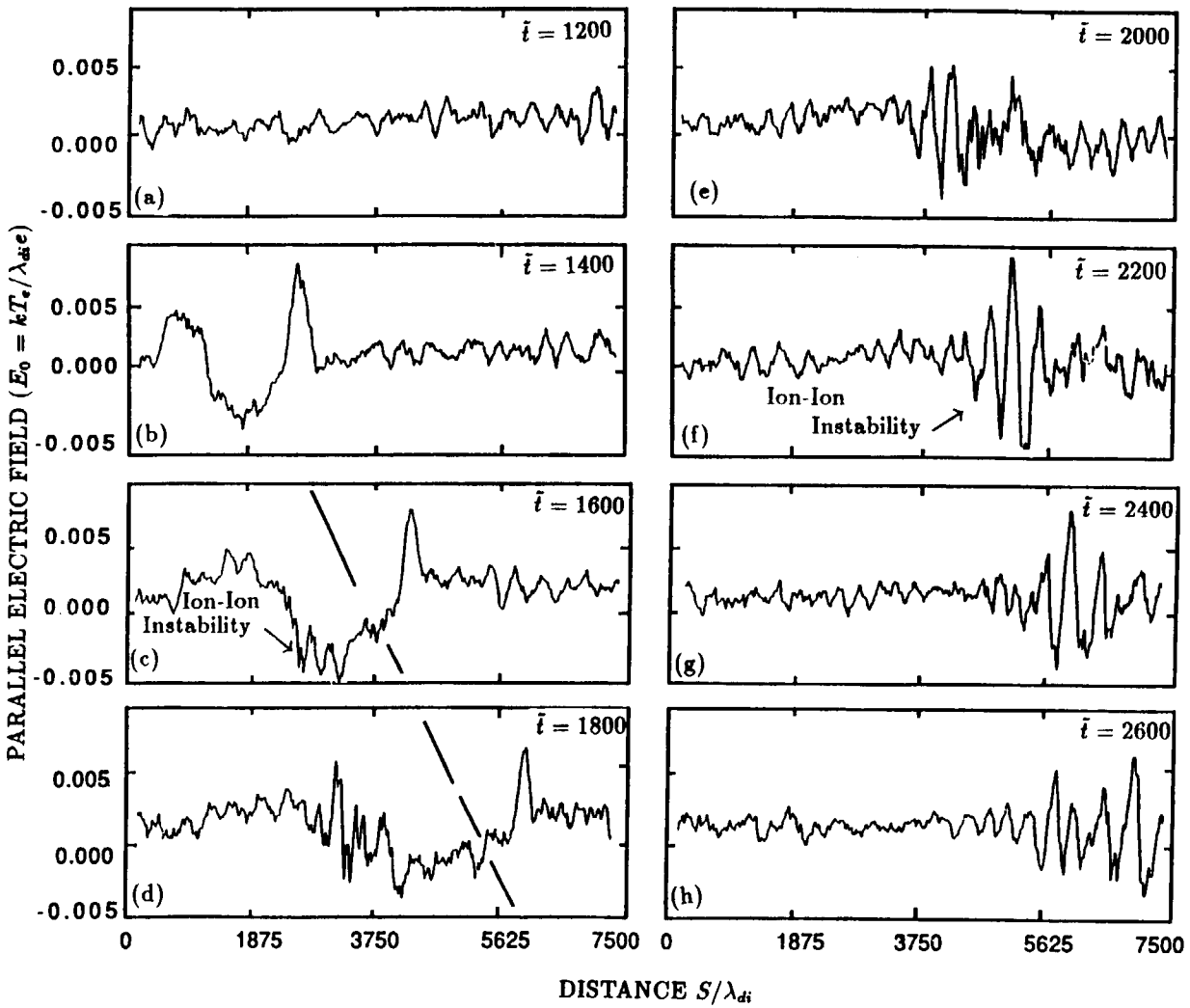
$\tilde{t} = 1200$
$\tilde{t} = 2000$
$\tilde{t} = 1400$
$\tilde{t} = 2200$
$\tilde{t} = 1600$
$\tilde{t} = 2400$
$\tilde{t} = 1800$
$\tilde{t} = 2600$
(a)
(b)
(c)
(d)
(e)
(f)
(g)
(h)
Ion-Ion Instability
Ion-Ion Instability
0.005
0.000
-0.005
0
1875
3750
5625
7500
PARALLEL ELECTRIC FIELD ($E_0 = kT_e/\lambda_{de}e$)
DISTANCE S/λ_{di}

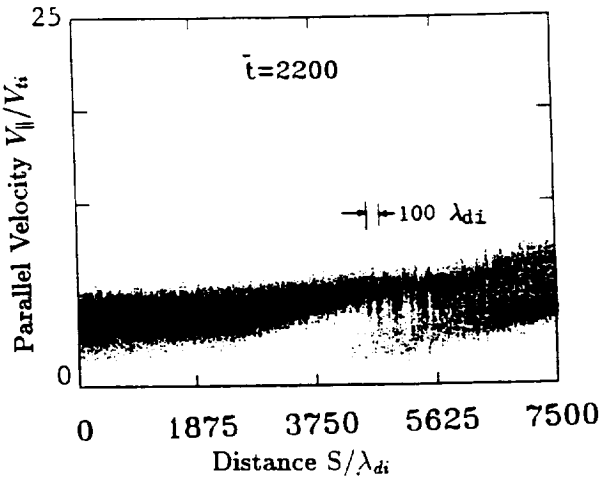
25
t=2200
100 λdi
0
0
1875
3750
5625
7500
Parallel Velocity $V_{\parallel}/V_{ti}$
Distance S/λ_{di}

Fig. 7

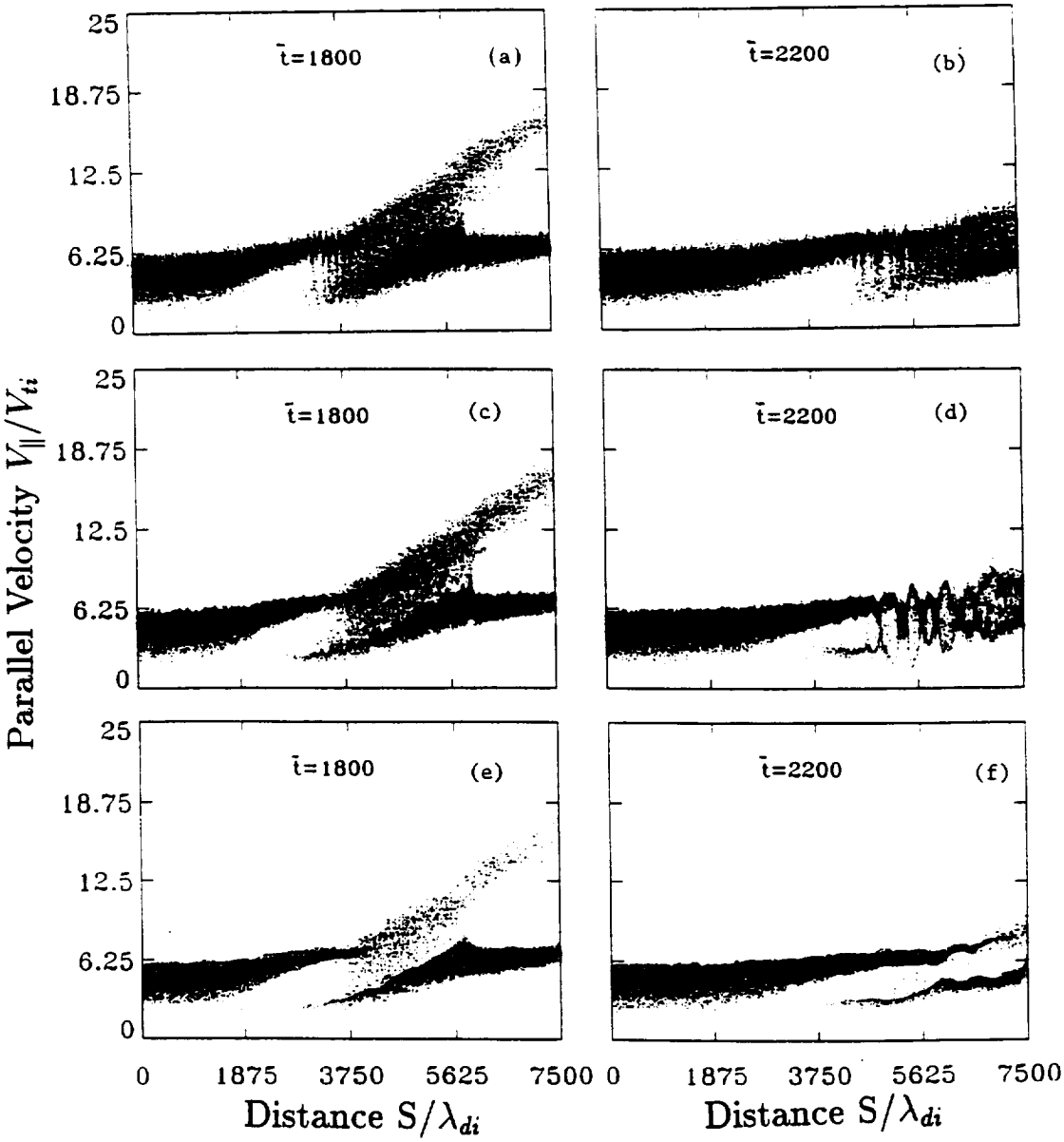
25
18.75
12.5
6.25
0
t̄=1800
(a)
t̄=2200
(b)
t̄=1800
(c)
t̄=2200
(d)
t̄=1800
(e)
t̄=2200
(f)
Parallel Velocity $V_{\parallel}/V_{ti}$
0
1875
3750
5625
7500
Distance S/λ_{di}

Fig. 8